Proton Collective Quantum Tunneling Induces Anomalous Thermal Conductivity of Ice under Pressure

Yufeng Wang,[1,2,*] Ripeng Luo,[2,*] Jian Chen,[3] Xuefeng Zhou,[3] Shanmin Wang,[3] Junqiao Wu,[4,5] Feiyu Kang,[1,2] Kuang Yu,[1,2,†] and Bo Sun[1,2,‡]

[1]*Tsinghua Shenzhen International Graduate School, Tsinghua University, Shenzhen 518055, China*
[2]*Tsinghua-Berkeley Shenzhen Institute, Tsinghua University, Shenzhen 518055, China*
[3]*Department of Physics and Academy for Advanced Interdisciplinary Studies, Southern University of Science and Technology, Shenzhen 518055, China*
[4]*Department of Materials Science and Engineering, University of California, Berkeley, California 94720, USA*
[5]*Materials Sciences Division, Lawrence Berkeley National Laboratory, Berkeley, California 94720, USA*

(Received 14 June 2023; revised 18 March 2024; accepted 20 May 2024; published 26 June 2024)

Proton tunneling is believed to be nonlocal in ice, but its range has been shown to be limited to only a few molecules. Here, we measured the thermal conductivity of ice under pressure up to 50 GPa and found it increases with pressure until 20 GPa but decreases at higher pressures. We attribute this nonmonotonic thermal conductivity to the collective tunneling of protons at high pressures, supported by large-scale quantum molecular dynamics simulations. The collective tunneling loops span several picoseconds in time and are as large as nanometers in space, which match the phonon periods and wavelengths, leading to strong phonon scattering at high pressures. Our results show direct evidence of global quantum motion existing in high-pressure ice and provide a new perspective to understanding the coupling between phonon propagation and atomic tunneling.

DOI: 10.1103/PhysRevLett.132.264101

As one of the most important substances in the Universe, ice challenges our understanding of its structures and properties, especially under extreme conditions, which are crucial in geological physics and environmental science [1–3]. In particular, the thermal conductivity (Λ) of pressurized ice plays an important role in the evolution and dynamics of icy planets, whose interior pressures range up to several hundred gigapascals (GPa) [4]. At such high pressures, the molecular structure of ice can be disrupted by hydrogen ion (proton) quantum tunneling, potentially affecting its thermal transport [5]. However, current data of Λ of compressed ice are available to a maximum pressure of only 22 GPa [6], showing a monotonic increase with pressure consistent with the classical Leibfried-Schlömann (LS) equation, while quantum effects in the dynamics of protons were obscure [7,8].

Meanwhile, ice has been an ideal model to study proton's quantum effects in the hydrogen bond network, which by themselves are long-standing and important topics in chemistry. Considering its simple molecular structure, ice features exceptionally complicated phase behavior under extreme conditions [9]. Specifically, at pressures higher than 2 GPa, the molecular crystal ice VII forms with an ordered oxygen (O) sublattice and a disordered hydrogen (H) sublattice. These sublattices are bounded by the "ice rule": Each O is covalently bonded to two H atoms which are hydrogen bonded to two other H_2O molecules (Fig. 1). Each H resides in a double-well potential, allowing it to locally tunnel between neighboring O sites and shuffle the position of the H sublattice. Theoretical analysis indicates that such tunneling events of different H atoms are coupled to each other due to the instability of certain charged defects that disrupt the ice rule [7,10], leading to a nonlocal quantum motion that induces the phase transition to ice X, an atomic (as opposed to molecular) crystal with symmetric hydrogen bonds. The transition is fundamentally different from normal thermodynamic phase transitions [11,12] and is related to numerous anomalies observed in high-pressure ice [13–16]. However, previous experiments probing proton tunneling in high-pressure ice are based on spectroscopic techniques, such as infrared [17] and nuclear magnetic resonance [18], which are sensitive only to the dynamics of single, isolated protons rather than collectively the entire hydrogen-bond network. A cryogenic scanning tunneling microscope (STM) overcomes the shortcomings of spectroscopic techniques and detects proton tunneling on a specific water tetramer system [19], but the tunneling range is limited to four protons. How long the collective quantum motions can travel is still an open question which has yet to be detected. And the dynamic phase transition modulated by the tunneling is much less studied.

Here, we report an anomalous, nonmonotonic pressure dependence of Λ of both H_2O and D_2O ice up to 50 GPa, in stark contrast to what the classical LS equation predicts. We show that such an anomaly is due to interactions between

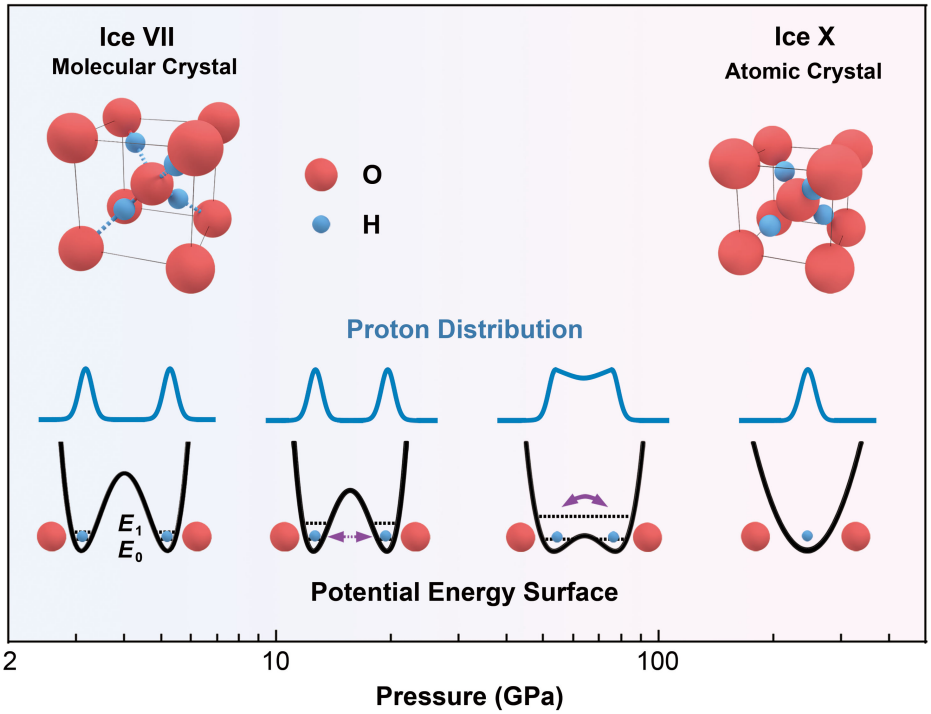

FIG. 1. Phase diagram of H_2O at room temperature and schematic of VII-X phase transition with proton symmetrization. The phase diagram is from a past report [9], and the boundary between ice VII and X remains controversial. The inset shows the structure of ice VII and ice X, as well as the potential energy of a proton situated between two oxygen atoms and proton distribution probability. E_0 and E_1 (black dashed lines) are the zero-point energy and first excited state of proton, respectively, and their difference represents the tunnel splitting. The purple lines represent the process of proton tunneling or hopping.

heat-carrying phonons and the proton tunneling, as the collective tunneling of multiple light atoms results in significant phonon scattering. Our work not only provides the widest range of thermal transport data for high-pressure ice, but also opens a new window to understanding its complicated phase diagram and phase transitions.

We measured Λ of ice under pressure using an *in situ* time-domain thermoreflectance (TDTR) system (Supplemental Material [20], Fig. S1). We put a thin sheet of metal-coated muscovite mica on the culet of diamond and then load liquid H_2O or D_2O into the diamond anvil cell. A 785 nm pump laser transmits through the diamond and ice to be focused onto the metal layer, where the laser beam is absorbed and converted into heat. The mica sheet is used as a thermal insulator, so that heat predominately flows into the surrounding ice rather than into the underlying diamond. A separate probe beam is used to monitor the temperature of the heated spot via the change of optical reflectance, and the resultant thermoreflectance signal is used to extract the thermal properties of ice. According to the sensitivity analysis of TDTR (Fig. S2 [20]), the thickness (h) and volumetric heat capacity (C_V) of the metal transducer are the main parameters introducing measurement uncertainty. Therefore, two different metal transducers, Al and $Au_{0.95}Pd_{0.05}$ (AuPd), were used separately to ensure the reliability of experimental results. In addition, we provide a detailed error analysis in Supplemental Material [20], which shows that our maximum experimental error is less than 30% at all pressures, thus ensuring the accuracy of experimental results. Λ of ice in Fig. 2 was obtained by fitting to the experimental data with a bidirectional thermal diffusion mode [6,41].

Below 20 GPa, Λ measured in this work increases monotonically, in excellent agreement with previous work and the LS equation (Figs. 2 and S3 [20]) [6]. However, beyond 20 GPa, we found that Λ decreases until 40 GPa and then starts to level off and slightly increase between 40 and 50 GPa, forming a second turning point. We believe that the measured Λ is intrinsic to ice due to the fact that the crystal grain size is much larger than the phonon mean free paths in ice, which is only a few nanometers (see Movie S1 in Supplemental Material [20] and our calculation below) and, thus, has minimum effect on thermal conductivity. As an electrical insulator [42,43], Λ of ice is completely dominated by lattice dynamics. It is well known that the lattice Λ in a crystal is proportional to the group velocity of acoustic phonons, heat capacity, and phonon lifetimes. Our *in situ* time-domain stimulated Brillouin scattering data (Fig. S4 [20]) indicates that the acoustic phonon velocity near the Γ point steadily increases over the entire pressure range we have studied. The heat capacity of ice VII is quite constant with a deviation of less than 30% in the entire

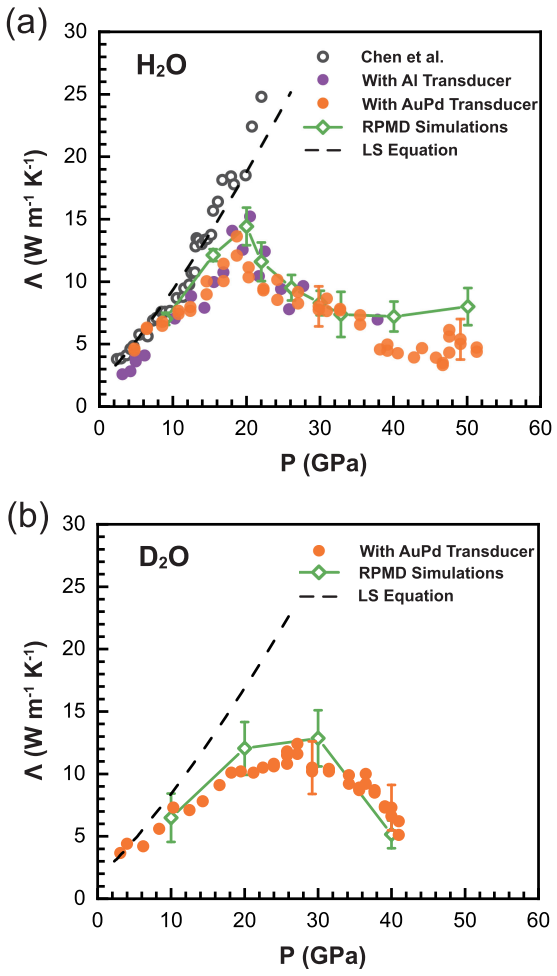

FIG. 2. Thermal conductivity of (a) H_2O and (b) D_2O under hydrostatic pressure. The purple and orange circles are TDTR results in this study with Al and AuPd transducer, respectively. The green line is results of RPMD simulations. The black dashed line is calculated with the classical LS equation [6]. The details of calculating measurement uncertainties are in Supplemental Material [20].

pressure range (Fig. S5 [20]). Therefore, the anomalous behavior of Λ we observed in ice must result from a new scattering mechanism arising above 20 GPa that strongly reduces the phonon lifetimes. The quantum nature of the new scattering mechanism is clearly evidenced by comparing Λ of H_2O ice with that of D_2O ice, which shows a similar trend but with the first turning point happening at about 10 GPa higher than H_2O [Fig. 2(b)]. Such a strong isotope effect points out the connection between the anomaly of Λ and the quantum proton tunneling in the ice VII lattice, as heavier particles have a lower tunneling probability.

In order to understand the mechanism behind the anomalous behavior of Λ, large-scale equilibrium quantum molecular dynamics (MD) simulations were performed. A reactive machine learning potential was trained using the DeepMD-kit [44] at the Perdew-Burke-Ernzerhof level of theory, and ring-polymer molecular dynamics (RPMD) [45] was used to propagate the dynamics. RPMD was proved to give a reliable description of both the thermodynamics and dynamics of short-living phonons in ice [46]. Both ice VII and X are isotropic, so the computed Λ are averaged over three directions and plotted along the side with the experimental data in Fig. 2, showing quantitative agreement between them. In order to eliminate the influence of thermal hopping, we also used classical MD to calculate the thermal conductivity of high-pressure ice, and the results are shown in Fig. S6 [20]. Our simulation results indicate that the impact of thermal hopping on thermal conductivity is limited at low pressure and becomes significant above 50 GPa. Therefore, the observed experimental results at 20 GPa are dominated by quantum effects. We further present the integrated heat flux time correlation functions (TCFs) for H_2O ice at different pressures (Fig. S7 [20]), combined with the integrated TCFs from the O sublattice only. Comparing the total and the O integrated TCFs, it is clear that, before 40 GPa, Λ is primarily contributed by the O sublattice. Therefore, the heavy O phonons are the main heat carriers before 40 GPa,

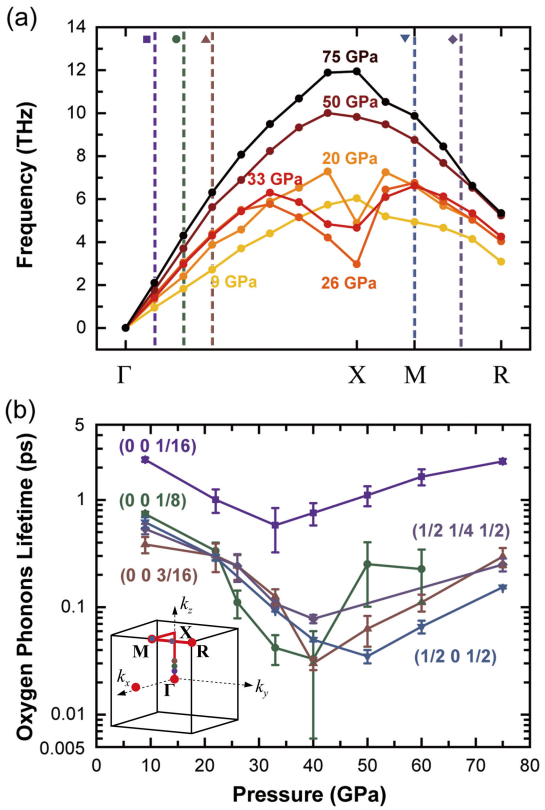

FIG. 3. (a) Pressure dependence of phonon dispersion. We show only a branch of acoustic mode for clarity. (b) Pressure dependence of typical phonon lifetime. The positions of the phonons in the reciprocal space are also labeled in (a) with dashed lines. The inset is the first Brillouin zone of the oxygen sublattice.

after which the H contribution rises as a consequence of the phonons propagating in the newly formed symmetrized H sublattice. The proton distribution profiles presented in Fig. S8 [20] support this picture, as the distinctive dual peaks start to merge at 40–50 GPa. Therefore, the second turning point of Λ observed at about 40 GPa is directly related to the beginning of proton symmetrization and the phase transition to ice X.

With the O phonons identified as the main heat carrier, the first turning point at 20 GPa can be attributed to the scattering of the O phonons by the tunneling protons. We performed lattice dynamics analysis on the O sublattice, using the Green's function method [47,48]. The dispersion relations and the lifetimes of several selected O phonons are shown in Figs. 3 and S9 [20]. At the vicinity of the Γ point, the group velocities gradually increase with pressure. It is consistent with the Brillouin scattering results (Fig. S4 [20]) and also matches the common wisdom, as higher density usually leads to stronger force constants. However, the frequencies near the X point exhibit a reverse trend, downshifting between 20 and 40 GPa, which, as we will explain later, is a direct result of the charged defects caused by proton tunneling. Moreover, O phonon lifetimes in all points decrease steadily before 30–40 GPa, indicating that the O phonons are strongly scattered by the proton tunneling events [Fig. 3(b)]. We found that lifetime at the X point (Fig. S10 [20]) is unstable, which is probably related to the phonon softening.

To gain a deeper insight, we analyzed the tunneling pattern and found that the tunneling events are highly coupled and form a series of closed loops with varying sizes, as shown in Figs. 4 and S11 [20]. Movie S2 [20] illustrates quantum tunneling loops of MD trajectory. The concentration of charge defects increases rapidly with pressure above 20 GPa (Fig. S12 [20]). The time and spatial scales of these tunnel loops also show strong pressure dependence. Between 20 and 30 GPa, the protons still feature a far-separated dual peak distribution (Figs. 1 and S8 [20]), indicating a thermally inaccessible barrier between the two sites. However, quantum tunnel loops spanning several picoseconds in time and as large as nanometers in space [Fig. 4(c)] can already be frequently observed. These values match the periods and wavelengths of the O phonons and cause strong phonon scattering, explaining the anomalous trend of Λ in the corresponding pressure range. Above 30 GPa, the tunneling rate becomes too high and starts to be decoupled with the O phonons on the timescale. Especially, tunneling counts decrease in the low-frequency region below 2 THz [Fig. 4(b)], where phonons with large group velocities contribute to the majority of Λ. As a result, the lifetime of long-wavelength O phonons [e.g., the one at $(0\,0\,1/16)$] begins to recover after 30 GPa [Fig. 3(b)].

Previous analysis indicated that, in ice VII, protons tunnel in a synchronized fashion within six-membered rings [10,49]. In this work, with a much larger simulation

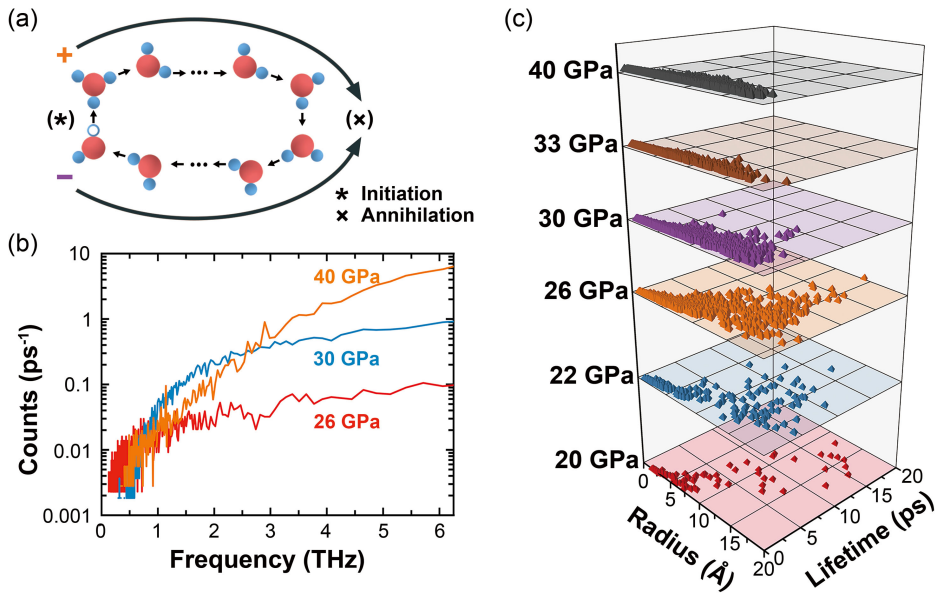

FIG. 4. (a) Schematic illustration of a collective tunneling loop. The tunneling of a proton occurs by excitation of charge defects (a pair of H_3O^+ and OH^-). The charge defect pair exhibits dominolike migrations along the loop with more proton tunneling events until being annihilated at the other side of the loop. We define the radius of the collective tunneling loop to be the geometrically effective radius of the tunneling path and the lifetime of the collective tunneling loop to be the time between the excitation and the annihilation of the charge defects. (b) Statistics of tunneling frequency at different pressures in H_2O. The tunneling frequency is the inversion of the lifetime. We show only tunneling frequency less than k_BT with T of 300 K, where most heat-carrying phonons lie. (c) Pressure dependence of the collective tunneling loops statistics in H_2O.

box, we find the collective tunneling happens over a larger spatial range and is not completely synchronized. At 300 K, many tunneling events are sequentially coupled via short-living ionic configurations, as indicated by previous studies [7]. The charged defects arising from the proton tunneling diffuse rapidly before being annihilated, forming large tunneling loops involving up to tens of molecules along the path. The O phonons with long wavelengths (∼ nanometers) and periods (∼ picoseconds) can be significantly scattered only by such collective tunneling loops instead of by single tunneling events previously detected by spectroscopy experiments (which typically happens in femtoseconds). The charged defects are also responsible for the abnormally softened phonons at the X point [Fig. 3(a)]. As shown in Fig. S13 [20], the mode at the X point is a collective vibration of two separate and interpenetrated hydrogen bond networks. At high densities, it is the only mode that is completely dominated by the nonbonding repulsion between O atoms. Since the diffusion of the charged defects is at a similar timescale to the O lattice vibration, their charge distribution can respond to the phonon vibrations concurrently. As a result, the electrostatic attraction between charged defects in the two networks softens the O─O repulsion, leading to the anomaly around the X point. This can also explain anomalous symmetry reduction that was also observed in pressure-dependence peak widths of Raman vibration mode $\nu_1(A_{1g})$ in past Raman spectroscopic studies [14,50–52] and splitting in some of the cubic diffraction peaks in x-ray diffraction experiments [51,53]. Past neutron diffraction observed an increase in translational motion of hydrogen under pressure [16], which is also consistent with our observation of increased proton collective motion. Recently, Tsuchiya *et al.* [54] reported that quantum tunneling may dominate at pressures exceeding 40 GPa based on elastic constant calculations. The difference in pressures is not ascribed to the computational method but to the physical properties. While elastic constant is sensitive to the formation of dynamically disordered phases, thermal conductivity in our case is subject to long-range tunneling loops with large distribution and enduring lifetime, which starts at 20 GPa according to our analysis. Conversely, in order to probe the global proton tunneling, the experiment tools must be sensitive to the corresponding temporal and spatial scales. Conventional methods to probe proton tunneling, such as incoherent quasielastic neutron scattering [55,56], are fast enough to detect proton tunneling but with limited ability to probe long-distance proton motion. STM [19] currently observed only the collective motion of four protons due to the limit of spatial resolution. On the contrary, thermal transport, as a diffuse phenomenon, is a naturally powerful tool to probe and reveal the global proton motions, as long as they match the time and length scales of heat-carrying phonons.

Our study is the first to demonstrate the collective quantum motion of protons occurring in a high-pressure, high-density phase of ice. The collective tunneling under high pressure yields a new perspective to explore the ice VII-X phase transition. Moreover, the analysis of coupling between the O phonons and proton tunneling deepens our understanding of the scattering mechanism between acoustic phonons and atomic tunneling that is only scarcely demonstrated previously. The thermal conductivity of ice we measured over a wider range of pressures also provides an important benchmark in the study of the evolution and internal dynamics of icy planets. Our results suggest that the thermal conductivity of ice is lower by an order of magnitude than previously estimated using classical models. Therefore, a lower thermal conductivity would imply slower heat transfer within the ice, leading to steeper temperature gradients, which might influence interactions between the rocky and icy layers and alter the planet's geological and topographical features [57].

The authors thank Dr. Fang Liu and Professor Xinqiang Wang from Peking University for depositing AuPd films. B. S. acknowledges support from National Natural Science Foundation of China-Israel Science Foundation Joint Scientific Research Program under Grant No. 52161145502, National Science Foundation of China under Grant No. 12004211, Shenzhen Science and Technology Program Grants No. RCYX20200714114643187 and No. WDZC20200821100123001, and Tsinghua Shenzhen International Graduate School Grants No. QD2021008N and No. JC2021008. K. Y. acknowledges support from National Natural Science Foundation of China under Grant No. 22103048 and Tsinghua Shenzhen International Graduate School under Grant No. HW2020009. J. W. acknowledges support from the U.S. Department of Energy, Office of Science, Office of Basic Energy Sciences, Materials Sciences and Engineering Division under Contract No. DE-AC02-05-CH11231 (EMAT program KC1201).

*These authors contributed equally to this letter.
†yu.kuang@sz.tsinghua.edu.cn
‡sun.bo@sz.tsinghua.edu.cn

[1] W. Nellis, D. Hamilton, N. Holmes, H. Radousky, F. Ree, A. Mitchell, and M. Nicol, Science **240**, 779 (1988).
[2] C. Cavazzoni, G. L. Chiarotti, S. Scandolo, E. Tosatti, M. Bernasconi, and M. Parrinello, Science **283**, 44 (1999).
[3] C. R. Bina and A. Navrotsky, Nature (London) **408**, 844 (2000).
[4] W. B. Hubbard, Science **275**, 1279 (1997).
[5] B. Sun, S. Niu, R. P. Hermann, J. Moon, N. Shulumba, K. Page, B. Zhao, A. S. Thind, K. Mahalingam, J. Milam-Guerrero *et al.*, Nat. Commun. **11**, 6039 (2020).
[6] B. Chen, W.-P. Hsieh, D. G. Cahill, D. R. Trinkle, and J. Li, Phys. Rev. B **83**, 132301 (2011).

[7] L. Lin, J. A. Morrone, and R. Car, J. Stat. Phys. **145**, 365 (2011).
[8] J. A. Morrone, L. Lin, and R. Car, J. Chem. Phys. **130**, 204511 (2009).
[9] L. Zhang, H. Wang, R. Car, and E. Weinan, Phys. Rev. Lett. **126**, 236001 (2021).
[10] C. Drechsel-Grau and D. Marx, Phys. Rev. Lett. **112**, 148302 (2014).
[11] M. Merolle, J. P. Garrahan, and D. Chandler, Proc. Natl. Acad. Sci. U.S.A. **102**, 10837 (2005).
[12] Q.-J. Ye, L. Zhuang, and X.-Z. Li, Phys. Rev. Lett. **126**, 185501 (2021).
[13] K. Umemoto, E. Sugimura, S. De Gironcoli, Y. Nakajima, K. Hirose, Y. Ohishi, and R. M. Wentzcovitch, Phys. Rev. Lett. **115**, 173005 (2015).
[14] C.-S. Zha, J. S. Tse, and W. A. Bassett, J. Chem. Phys. **145**, 124315 (2016).
[15] N. Noguchi and T. Okuchi, J. Chem. Phys. **144**, 234503 (2016).
[16] K. Komatsu, S. Klotz, S. Machida, A. Sano-Furukawa, T. Hattori, and H. Kagi, Proc. Natl. Acad. Sci. U.S.A. **117**, 6356 (2020).
[17] A. Goncharov, V. Struzhkin, M. Somayazulu, R. Hemley, and H.-K. Mao, Science **273**, 218 (1996).
[18] T. Meier, S. Petitgirard, S. Khandarkhaeva, and L. Dubrovinsky, Nat. Commun. **9**, 2766 (2018).
[19] X. Meng, J. Guo, J. Peng, J. Chen, Z. Wang, J.-R. Shi, X.-Z. Li, E.-G. Wang, and Y. Jiang, Nat. Phys. **11**, 235 (2015).
[20] See Supplemental Material at http://link.aps.org/supplemental/10.1103/PhysRevLett.132.264101, which includes Refs. [21–40], for experimental details and simulation methods.
[21] A. Dewaele, M. Torrent, P. Loubeyre, and M. Mezouar, Phys. Rev. B **78**, 104102 (2008).
[22] S. Raghavan, P. Imbrie, and W. A. Crossley, Appl. Spectrosc. **62**, 759 (2008).
[23] A. Feldman *et al.*, High Temp.—High Press. **31**, 293 (1999).
[24] X. Xie, J. M. Dennison, J. Shin, Z. Diao, and D. G. Cahill, Rev. Sci. Instrum. **89**, 104904 (2018).
[25] W.-P. Hsieh, B. Chen, J. Li, P. Keblinski, and D. G. Cahill, Phys. Rev. B **80**, 180302(R) (2009).
[26] S. R. Shieh, W.-P. Hsieh, Y.-C. Tsao, C. Crisostomo, and H. Hsu, J. Geophys. Res. Planets **127**, e2022JE007180 (2022).
[27] G. T. Hohensee, R. Wilson, and D. G. Cahill, Nat. Commun. **6**, 6578 (2015).
[28] R. G. Greene, H. Luo, and A. L. Ruoff, Phys. Rev. Lett. **73**, 2075 (1994).
[29] K. Takemura and A. Dewaele, Phys. Rev. B **78**, 104119 (2008).
[30] N. Curetti, D. Levy, A. Pavese, and G. Ivaldi, Phys. Chem. Miner. **32**, 670 (2006).
[31] L. Zhang, J. Han, H. Wang, W. Saidi, R. Car *et al.*, *Advances in Neural Information Processing Systems* (Curran, Red Hook, 2018), p. 4436.
[32] V. Kapil, M. Rossi, O. Marsalek, R. Petraglia, Y. Litman, T. Spura, B. Cheng, A. Cuzzocrea, R. H. Meißner, D. M. Wilkins *et al.*, Comput. Phys. Commun. **236**, 214 (2019).
[33] M. Ceriotti, M. Parrinello, T. E. Markland, and D. E. Manolopoulos, J. Chem. Phys. **133**, 124104 (2010).
[34] L. Ercole, A. Marcolongo, and S. Baroni, Sci. Rep. **7**, 15835 (2017).
[35] C. Campana and M. H. Müser, Phys. Rev. B **74**, 075420 (2006).
[36] A. J. McGaughey and J. M. Larkin, Annu. Rev. Heat Transf. **17**, 49 (2014).
[37] T. M. Yamamoto, J. Chem. Phys. **123**, 104101 (2005).
[38] A. Polian and M. Grimsditch, Phys. Rev. Lett. **52**, 1312 (1984).
[39] M. Ahart, M. Somayazulu, S. A. Gramsch, R. Boehler, H.-k. Mao, and R. J. Hemley, J. Chem. Phys. **134**, 124517 (2011).
[40] Z. M. Grande, C. H. Pham, D. Smith, J. H. Boisvert, C. Huang, J. S. Smith, N. Goldman, J. L. Belof, O. Tschauner, J. H. Steffen *et al.*, Phys. Rev. B **105**, 104109 (2022).
[41] D. G. Cahill, Rev. Sci. Instrum. **75**, 5119 (2004).
[42] T. Okada, T. Iitaka, T. Yagi, and K. Aoki, Sci. Rep. **4**, 1 (2014).
[43] B. Liu, Y. Gao, Y. Han, Y. Ma, and C. Gao, Phys. Lett. A **380**, 2979 (2016).
[44] H. Wang, L. Zhang, J. Han, and E. Weinan, Comput. Phys. Commun. **228**, 178 (2018).
[45] S. Habershon, D. E. Manolopoulos, T. E. Markland, and T. F. Miller III, Annu. Rev. Phys. Chem. **64**, 387 (2013).
[46] R. Luo and K. Yu, J. Chem. Phys. **153**, 194105 (2020).
[47] L. T. Kong, G. Bartels, C. Campana, C. Denniston, and M. H. Müser, Comput. Phys. Commun. **180**, 1004 (2009).
[48] L. T. Kong, Comput. Phys. Commun. **182**, 2201 (2011).
[49] F. Trybel, M. Cosacchi, T. Meier, V. M. Axt, and G. Steinle-Neumann, Phys. Rev. B **102**, 184310 (2020).
[50] P. Pruzan, J. Chervin, and M. Gauthier, Europhys. Lett. **13**, 81 (1990).
[51] P. Pruzan, J. Chervin, E. Wolanin, B. Canny, M. Gauthier, and M. Hanfland, J. Raman Spectrosc. **34**, 591 (2003).
[52] H. Hirai, H. Kadobayashi, T. Matsuoka, Y. Ohishi, and Y. Yamamoto, High Press. Res. **34**, 289 (2014).
[53] M. Somayazulu, J. Shu, C.-s. Zha, A. F. Goncharov, O. Tschauner, H.-k. Mao, and R. J. Hemley, J. Chem. Phys. **128**, 064510 (2008).
[54] J. Tsuchiya, M. Shiga, S. Tsuneyuki, and E. C. Thompson, arXiv:2307.14214 [Phys. Rev. Res. (to be published)].
[55] L. E. Bove, S. Klotz, A. Paciaroni, and F. Sacchetti, Phys. Rev. Lett. **103**, 165901 (2009).
[56] A. I. Kolesnikov, G. Ehlers, E. Mamontov, and A. Podlesnyak, Phys. Rev. B **98**, 064301 (2018).
[57] D. W. Meyer, W.-P. Hsieh, H. Hsu, C.-Y. Kuo, and J.-F. Lin, J. Geophys. Res. Planets **127**, e2021JE007059 (2022).